Implementation of PSF Engineering in High-Resolution 3D Microscopy Imaging with a LCoS (Reflective) SLM

Sharon V. King[1], Ana Doblas[2], Nurmohammed Patwary[1], Genaro Saavedra[2], Manuel Martínez-Corral[2], Chrysanthe Preza[1♦]

[1]Department of Electrical and Computer Engineering, the University of Memphis, Memphis, TN 38152, USA

[2]3D Imaging and Display Laboratory University of Valencia, Department of Optics, E-46100 Burjassot, Spain

ABSTRACT

Wavefront coding techniques are currently used to engineer unique point spread functions (PSFs) that enhance existing microscope modalities or create new ones. Previous work in this field demonstrated that simulated intensity PSFs encoded with a generalized cubic phase mask (GCPM) are invariant to spherical aberration or misfocus; dependent on parameter selection. Additional work demonstrated that simulated PSFs encoded with a squared cubic phase mask (SQUBIC) produce a depth invariant focal spot for application in confocal scanning microscopy. Implementation of PSF engineering theory with a liquid crystal on silicon (LCoS) spatial light modulator (SLM) enables validation of WFC phase mask designs and parameters by manipulating optical wavefront properties with a programmable diffractive element. To validate and investigate parameters of the GCPM and SQUBIC WFC masks, we implemented PSF engineering in an upright microscope modified with a dual camera port and a LCoS SLM. We present measured WFC PSFs and compare them to simulated PSFs through analysis of their effect on the microscope imaging system properties. Experimentally acquired PSFs show the same intensity distribution as simulation for the GCPM phase mask, the SQUBIC-mask and the well-known and characterized cubic-phase mask (CPM), first applied to high NA microscopy by Arnison *et al.*[10], for extending depth of field. These measurements provide experimental validation of new WFC masks and demonstrate the use of the LCoS SLM as a WFC design tool. Although efficiency improvements are needed, this application of LCoS technology renders the microscope capable of switching among multiple WFC modes.

KEYWORDS: Microscopy, wave-front encoding, spatial light modulators, liquid crystal

1. INTRODUCTION

WFC has been successfully applied, beyond the initial concept developed by Dowski and Cathy for extended depth of field (EDF) imaging[1], to create a variety of microscopy modes such as: super-resolved localization microscopy, using a double helix PSF[2]; spatial light interference microscopy (SLIM) using a time-varying Zernike phase contrast PSF[3] and spiral phase contrast microscopy using a differentiating PSF[4]. Recently, WFC PSFs engineered with a generalized cubic phase mask (GCPM)[5] and a squared cubic phase mask (SQUBIC)[6] have been shown insensitive to object induced spherical aberration (SA). Application of these engineered PSFs to optical sectioning microscopy (computational or confocal) has the potential to improve this process in images of thick samples (which suffer most from sample-induced SA).

Simulation studies of GCPM and SQUBIC phase masks applied to 3D microscope systems have made clear the importance of selecting the appropriate phase mask parameters[7,8]. In order to validate the influence of phase mask parameter choice on WFC PSF performance, a large number of phase masks must be implemented experimentally. For this study, a LCoS (LC for short) SLM was chosen as a more cost effective method of experimental investigation. Using

♦cpreza@memphis.edu; phone 1 901 678-4369; fax 1 901 678-5469; cirl.memphis.edu

Three-Dimensional and Multidimensional Microscopy: Image Acquisition and Processing XXI, edited by Thomas G. Brown, Carol J. Cogswell, Tony Wilson, Proc. of SPIE Vol. 8949, 894913

the LC SLM as a design tool also allows phase mask parameters to be changed or phase mask designs switched electrically without mechanical realignment of the optical system.

To experimentally observe engineered PSF properties, we implemented PSF engineering in a commercial, upright, Zeiss AxioImager microscope modified with a dual camera port and a LC SLM adapted to the second imaging path. We effectively measured the PSF by capturing images of unresolved fluorescent beads with a high NA objective.

This paper provides new information on adaptation of the LC SLM to an upright microscope and its use in WFC PSF engineering for high-NA 3D microscopy. Section 2 briefly presents the theoretical form of the WFC phase masks: CPM, GCPM and SQUBIC and the need for WFC in optical sectioning microscopy. Section 3 describes methods used for the adaptation of the SLM to the microscope and experimental imaging methods as well as information relevant to the simulated WFC PSFs. Methods used for numerically computing simulations are discussed in detail in previous publications[5]. Section 4 presents results of the SLM implementation of the three WFC phase mask designs; the CPM, GCPM and the SQUBIC. These results include measurement of SLM implemented WFE PSFs and comparison of measured WFE PSFs with their simulated counterparts.

2. BACKGROUND

The background information here fulfills two purposes. One is to review the mathematical and theoretical background of the WFC phase masks being investigated. Another is to motivate the need for WFC in high NA 3D microscopy.

2.1 WFC phase masks: CPM, GCPM and SQUBIC

Wave-front coding techniques are used to manipulate phase and amplitude properties of the optical wave-front at the imaging system exit pupil and to create unique engineered point spread functions (PSFs)[1]. Methods of wave-front encoded phase mask design have been thoroughly discussed in the literature[9] . Dowski and Cathey describe this approach in detail with respect to application in extended depth of field and more generally as a new paradigm for imaging systems design[1].

The phase of the CPM used in this study, first applied to high NA microscopy by Arnison *et al.*[10], is given by:

$$CPM:\phi\left(f_x,f_y\right)=\alpha(f_x^3+f_y^3), \tag{1}$$

where f_x and f_y are the Cartesian co-ordinates across the pupil and α is the strength of the phase mask. This phase mask design was derived by finding an approximate solution, via the stationary phase method, to the ambiguity function of a general phase mask function for which the function is independent of phase delay[1].

An alternative approach to phase mask design optimizes image quality merit functions to select the parameters of a generalized polynomial expression[11], given by:

$$GCPM:\phi\left(f_x,f_y\right)=\alpha(f_x^3+f_y^3)+\beta(f_x^2 f_y+f_x f_y^2), \tag{2}$$

where α and β are design parameters. This approach has been used to select phase masks that improve upon the extended depth of focus characteristics of the CPM mask and that may decrease PSF depth variability due to sample induced SA[5]. Previous work demonstrated that simulated intensity PSFs encoded with a GCPM are invariant to either SA or misfocus[5]. Simulation studies predict that for parameters of α = 50 and β = -50, a 1.2NA imaging system will have a PSF; with an intensity distribution that varies with depth less than the PSF of an equivalent CCA imaging system. Alternatively, for parameters of α = 150 and β = -450, a 1.2NA imaging system will have a PSF; with an intensity distribution that extends the depth of field with less axial asymmetry than the CPM PSF.

A WFC phase mask designed specifically for reducing the impact of SA in microscopy was produced with yet another approach to WFC design. The design was derived from a model, formalized to assess the effect of SA in high NA optical systems. In this case, a squared cubic phase mask (SQUBIC) was produced and has been shown to create an invariant PSF in depth-scanning of thick samples for confocal scanning microscopy[6]. Its form is given by:

$$SQUBIC:\varphi(f_x,f_y)=A\left(\frac{\sqrt{1-(f_x^2+f_y^2)\sin^2\theta}-\cos\theta}{\cos\theta-1}+0.5\right)^3, \quad (3)$$

where A is a design parameter and θ is the maximum acceptance angle of imaging pupil.

2.2 PSF depth variability in 3D microscopy

3D microscopy methods use automation, digital detection and computational processing, and a variety of combinations of these, to capture high resolution images of a 3D volume. Sophisticated 3D microscopy methods employ techniques for improved isotropy of the resolution, particularly to increase the axial resolution. The most common methods for high resolution fluorescence imaging are optical sectioning either by confocal microscopy or by computational optical sectioning microscopy (COSM)[12].

The variability of the PSF as a function of depth from the coverslip introduces errors and artifacts in both confocal and COSM approaches. The dominant factor causing PSF depth variability is spherical aberration (SA) resulting from the mismatch between the refractive indices of mounting and immersion mediums[13]. SA and its effect on the PSF are depth dependent and they increase with depth of focus into the specimen, i.e. the characteristics of the out-of-focus light change with depth. Artifacts are created in COSM when these depth varying and object dependent characteristics are not rigorously modeled and in confocal optical sectioning when the increased blur requires increased laser excitation; eventually reaching signal to noise limitations or damaging the sample. Errors are also introduced in both optical sectioning methods because SA causes light to appear in focus at a plane other than its actual location[13].

3. METHODS

The following describes how the implementation of WFC was accomplished and how experimental measurements of WFC phase masks and WFC PSFs were acquired. The relevant details of the numerical computation of simulated WFC PSFs are also described.

3.1 The LC WFC microscope imaging path

PSF engineering was implemented by modifying a Zeiss AxioImager. This commercial upright, wide-field microscope system accommodates a dual camera port configuration, installed by Zeiss. The dual port configuration is created by inserting a mirror between the filter cube and the ocular housing. The mirror is mounted on a motorized mechanical stage that is automatically switched in or out of the optical path via software controls. The dual camera ports are fitted with the same model camera (Zeiss Axiocam MRm), effectively creating two imaging systems. One camera captures an image via the original microscope imaging path (referred to as Top in Fig. 1), while the other captures the LC WFC image.

The LC WFC imaging path was built by modifying the side camera port to incorporate the SLM. The camera image plane and the objective back-focal-plane are reimaged outside this port via a unit magnification, four-*f* imaging system[2]. This relay system is folded at the SLM, since the SLM does not transmit, so that light reflects from the SLM at a 20 deg angle. The LC layer of the SLM is mounted conjugate to the relayed objective back-focal plane. A linear polarizer is used to align the orientation of the illumination polarization with the optic axis of the LC layer. The AxioCam is mounted in the relayed image plane. In some cases, a small magnification or adjustable zoom may be introduced into the four-*f* imaging system so that the full pixel format of the SLM is illuminated by the exit pupil aperture and the full resolution of the SLM can be used to encode the pupil phase. However, since the aperture is round and the SLM is generally square or rectangular in format some comprise has to be made. In this study, no magnification was used. This approach was taken in order to allow direct comparison between conventional and WFC imaging, without a change in image scale.

The size of the digital phase mask pattern was matched to the magnification of the pupil at the SLM. The exit pupil of the 1.4-NA objective lens was imaged onto a 229x229 pixel area of the SLM. Each phase mask pattern was computed within a circular pupil aperture (on a 229 x 229 grid with spatial frequencies, f_x and f_y, ranging from [-1 to 1] over the 229 columns/rows). This grid was set inside a 512 x 512 grid required by the SLM format. The values of the numerical CPM, GCPM and SQUBIC masks were normalized and mapped in a range of 16 bits from 0 to 2π in order to project them on the SLM. The SLM (Boulder Nonlinear Systems), designed for 400-700 nm illumination at normal incidence, was used with a calibration created in situ for 532 nm illumination at 20 deg incidence.

3.2 Experimental WFC imaging

Experimental PSFs are measured by using unresolved fluorescent beads as an effective point source. This effective fluorescence source (λ_{peak} = 508-nm) emits from 0.175-μm-diameter beads (Invitrogen Point Source Kit, P7220). A dilute solution of beads was dried on the cover-slip and then mounted in the glycerol mounting medium (RI ~ 1.47) provided with the kit and a high-precision Zeiss cover slip. Individual beads were imaged with a 63x/1.4NA objective lens and a 515nm-565nm emission filter (Zeiss filter set 10). The size of the camera pixels is such that the effective experimental voxel size is 0.1 x 0.1 x 0.1 μm^3. The imaging system magnification and voxel size are the same as those of the simulated system.

3.3 Simulated WFC imaging

Simulated PSFs are computed numerically using a WFC imaging model. This model is a modified conventional model in which the generalized pupil function is given an additional phase term. Details of the mathematics of this model may be found in previous publication[13,5]. The imaging model was given system and environmental parameters that matched the experimental system as closely as possible to simulate its response as accurately as possible.

Simulated PSFs for conventional widefield microscopy were computed using the Gibson and Lanni PSF model[13] via the PSF computation module of the COSMOS package[14]. PSFs were computed on a 256 x 256 x 300 grid with voxels of size 0.1 x 0.1 x 0.1 μm^3. The system parameters used to image the point source are: a 63x/1.4 NA oil-immersion objective lens (RI = 1.515) and an emission wavelength λ = 515 nm. The environmental parameters are: a point source located at 25μm depth in glycerol (RI = 1.47) just below the coverslip. WFE-PSFs were calculated by first computing the 2-D Fourier transform of the complex-amplitude clear circular aperture (CCA) PSFs, thereby obtaining the conventional amplitude transfer function. At each focus depth, a 2D WFE-PSF was computed by applying the phase mask to the generalized pupil function and finally a 3D WFE-PSF was obtained by stacking the 2D WFE-PSFs. A mathematical description of this process is found in[5].

The distance of the simulated point source from the cover slip was chosen through a comparison study in which the depth variation of the simulated CCA PSF was related to the measured PSF acquired through the conventional microscope (Fig. 1). Although the experimental point sources are on the cover glass before mounting, their spherical surface may not remain in direct contact with the coverslip after mounting. Evidence of this possibility is seen in the axial asymmetry observed in the experimental CCA PSF which may be interpreted as an indicator of SA. Although the refractive index RI mismatch, Δn = 0.05, between the cover-glass and the immersion medium is expected to introduce some SA, the difference in axial asymmetry is more than predicted by simulation. Therefore, the appropriate depth parameter for simulation of the experimental point source can only be determined empirically by investigating the differences between normalized PSF intensity distributions at simulated depths in the range 15-40μm, and the experimental PSF intensity.

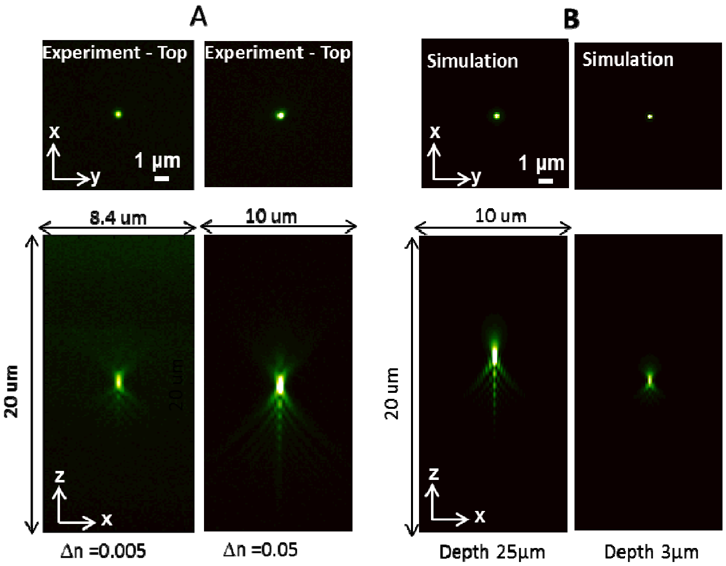

Fig. 1: Empirical determination of the point source depth used in the PSF simulation. In column A, the experimental CCA PSF (Δn = 0.005) emitted by beads dried on the coverslip mounted in UV cured optical cement, shows significantly less axial asymmetry than the experimental CCA PSF (Δn = 0.05) emitted by beads dried on the coverslip mounted in glycerol. In column B, the simulated CCA PSF (Δn = 0.05) at 25µm below the coverslip, shows an asymmetrical intensity spread in the axial direction that compares best with the experimental PSF measurement (Δn = 0.05). Simulated WFE and experimental PSFs are computed and acquired with a 63x, 1.4 NA lens and a 515nm wavelength.

4. RESULTS AND DISCUSSION

Experimentally measured WFC-PSFs show a 3D spatial intensity distribution that is comparable to the simulated intensity for the CPM, GCPM, and the SQUBIC phase masks. Although experimental properties of the WFC-PSFs are not in perfect agreement with those predicted by simulation (Fig. 2), they confirm basic properties of the PSF that are consistent with the function of the phase mask design. The largest observable differences between measured and simulated PSFs are the effects of experiment related noise and the influence of an intensity distribution that appears to be unmodulated during WFC.

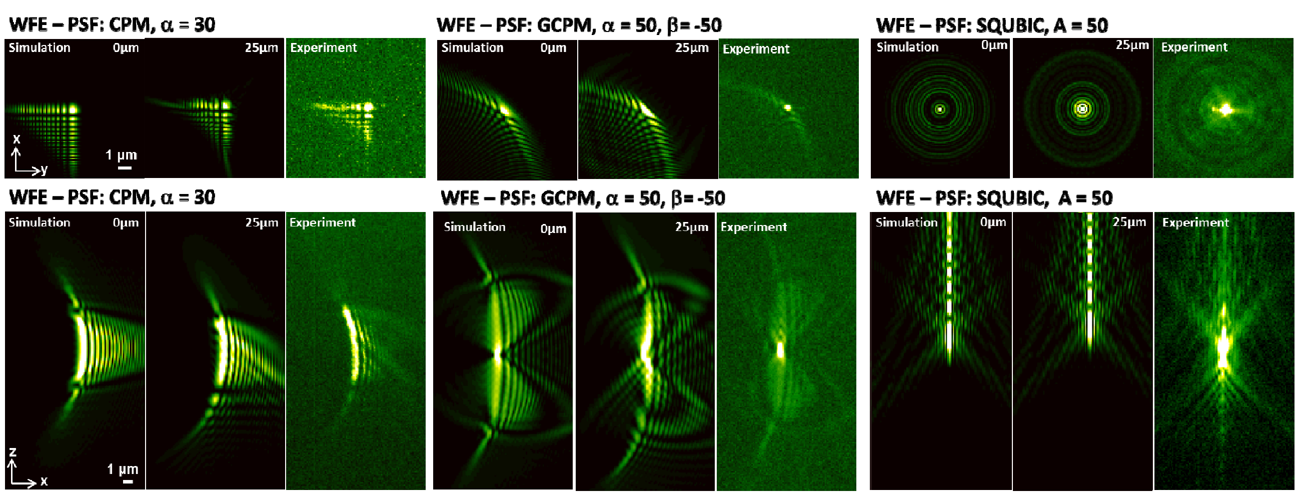

Fig. 2: Intensity of the 3D PSF shows good agreement between experiment and simulation at 25µm below the coverslip. Comparison of experiment with simulation at both 0µm and 25µm depths highlights the designed properties of the GCPM and SQUBIC WFC. Due to the low signal and low phase mask efficiency, experimental images are displayed using different intensity scales in order to show low-intensity details. The lateral view is shown at the best focus axial location. Simulated and experimental PSFs are computed and acquired with a 63x, 1.4 NA lens and a 515nm wavelength.

The CPM PSF (α= 30) curvature along the axial direction and away from the nominal focus, shown in simulation to cause inaccurate reconstruction of objects in lateral position[5], can also be seen in the experimental PSFs. Simulated CPM PSFs indicate the expected effect of SA, i.e., intensity asymmetry along Z, that results due to refractive index difference, $\Delta n = 0.05$, at the coverslip to mounting medium interface and the location of the point light source at 25 μm depth below the coverslip. The measured CPM PSFs show comparable effects visible in the XY view (Fig. 2, top row) in the curvature of the extreme ends of the lateral intensity pattern and in the XZ view (Fig. 2, bottom row) in the asymmetric axial variation of the lateral intensity pattern. The impact of these SA effects is a degradation of the extended depth of field.

The GCPM PSF (parameters α= 50, α= -β), in contrast, is produced by a phase mask design selected to balance sensitivity to misfocus with insensitivity to SA[5]. These PSF properties are proposed to enhance COSM. In fact, the measured GCPM PSF, acquired with a point source at the same depth as the CPM PSF, shows that SA has significantly less effect on its shape than the CPM or CCA PSFs (see Fig. 1). Axial asymmetry of the GCPM PSF is significantly less pronounced than that of the both CPM and CCA PSFs, in both simulation and experiment. The experimental GCPM PSF shows less axial asymmetry than simulation, which may be attributed to its low signal-to-noise ratio. As a result of noise, very low magnitude diffraction effects are not discernible experimentally. However, the scale and spatial variance of the measured diffraction pattern is exactly predicted by simulation. Simulated and experimental GCPM PSFs exhibit a decreasing axial intensity away from its central peak that characterizes sensitivity to misfocus. Both also show an increasingly large lateral extent of the PSF with increasing amount of misfocus. This property demonstrates the reduced depth of field of this particular GCPM PSF as compared to the CPM PSF.

The SQUBIC PSF (*A* =50) is also proposed to enhance optical sectioning microscopy, but with different properties. The experimental SQUBIC PSF confirms the lateral confinement of the very brightest part of the simulated SQUBIC PSF intensity. The experimental SQUBIC PSF is axially asymmetric and appears to have at least one minimum between a primary area of brightest intensity and a second area of bright intensity. This asymmetry is consistent with the simulated SQUBIC PSF that has a very long axial intensity distribution, punctuated by multiple nulls. The lateral intensity confinement renders the PSF very robust to SA. For these simulation parameters, it is almost completely invariant with the changes in SA. The axial asymmetry of its shape distinguishes this PSF from the CPM and GCPM PSFs and makes it an unsuitable for EDF microscopy.

The GCPM PSF (parameters α= 150, β= -3α) was selected, and demonstrated in simulation, as a generalization of the CPM design that can be also used to extend the depth of field of the imaging system. It produces a PSF for EDF without curvature along the axial direction. Unfortunately, this phase mask has a rapidly varying phase that cannot be efficiently implemented with the SLM. Nevertheless a GCPM design with parameters α= 30, β= -3α, validates that an EDF PSF is produced with this design without the curvature of the CPM PSF (Fig. 3).

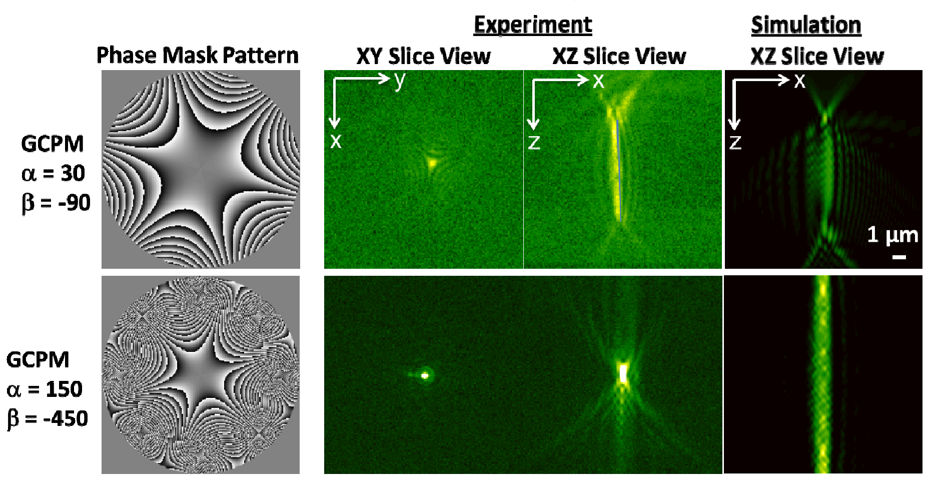

Fig. 3: EDF with GCPM could be validated only for low values of the design parameters of α and β. Comparison of experiment with simulation at 25μm depth shows good agreement for GCPM with α= 30, α= -3β. The length of the brightest part of the PSF for α= 30, α= -3β, is roughly 7μm. For GCPM with α= 150, α= -3β the experimental PSF intensity appears largely unmodulated by WFC.

A portion of the disparity between simulated and experimental PSFs can be attributed to a low signal to noise ratio due to the small size of the fluorescent point source. However, error due to infidelity of the mask implementation must also be considered. A mismatch between the numerical phase mask applied to the SLM and the actual WFC SLM phase can occur for several possible reasons. For example, it is known that the SLM is limited in the spatial frequency with which it can resolve 0 and 2π phase modulation depth[15]. In addition, others have shown that LC SLM may exhibit a frequency dependent decrease in efficiency[16]. We are currently investigating the role of these properties in our implementation and their effect on WFC PSF engineering. We will report on this elsewhere.

5. CONCLUSION

Incorporation of liquid crystal technologies into the microscope imaging path is a potential method to provide switchable WFC capability in a high NA microscope. The LC SLM WFC microscope described in this paper exhibited WFC PSFs which validated previously published simulation studies of WFC PSFs for 3D microscopy. The properties exhibited by experimentally measured WFC-PSFs agree with the predictions of WFC-PSFs simulated using conventional imaging models. With some practical limitations, the experimental LC SLM WFC phase masks can successfully implement a wide range of WFC phase function designs for validation and investigation of WFC design parameters. Still, improvement of the efficiency of this implementation approach is needed and further investigation of the fidelity with which the phase masks can be implemented with the LC SLM is underway.

ACKNOWLEDGEMENT

This work is supported by the National Science Foundation (NSF CAREER award DBI-0844682 and NSF IDBR award DBI-0852847, PI: C. Preza) and the University of Memphis. Additionally, AD, GS and MM-C want to acknowledge the financial support of Ministerio de Economía (grant DPI2012-32994) and Generalitat Valenciana (grant PROMETEO/2009/077), Spain.

REFERENCES

[1] Cathey, W. T. and Dowski, E. R., "New Paradigm for Imaging Systems," Appl. Opt. 41, 6080-6092 (2002).

[2] Pavani, S. R. P. and Piestun, R., "Three dimensional tracking of fluorescent microparticles using a photon-limited double-helix response system," Opt. Express 16, 22048–22057 (2008).

[3] Wang, Z., Millet, L., Mir, M., Ding, H., Unarunotai, S., Rogers, J., Gillette, M. U. and Popescu, G., "Spatial light interference microscopy (SLIM)," Optics Express 19, 1016-1026 (2011).

[4] Bernet, S., Jesacher, A., Fürhapter, S., Maurer, C., and Ritsch-Marte, M., "Quantitative imaging of complex samples by spiral phase contrast microscopy," Opt. Express 14, 3792-3805 (2006).

[5] Yuan, S. and Preza., "Point-spread function engineering to reduce the impact of spherical aberration on 3D computational fluorescence microscopy imaging," Opt. Express 19, 23298-23314 (2011).

[6] Saavedra, G., Escobar, I., Martinez-Cuenca, R., Sanchez-Ortiga, E., and Martínez-Corral, M., "Reduction of spherical-aberration impact in microscopy by wavefront coding," Optics Express 17, 13810–13818 (2009).

[7] Doblas, A., King, S. V., Patwary, N., Saavedra, G., Martinez-Corral, M., and Preza, C., "Investigation of the SQUBIC phase mask design for depth-invariant widefield microscopy point-spread function engineering," submitted Proc.SPIE, Three-Dimensional and Multidimensional Microscopy: Image Acquistion and Processing XX, (2014).

[8] Patwary, N., Doblas, A., King, S. V., and Preza, C., "Reducing depth induced spherical aberration by wavefront coding in 3D widefield fluorescence microscopy," submitted Proc.SPIE, Three-Dimensional and Multidimensional Microscopy: Image Acquistion and Processing XX, (2014).

[9] Dowski, E.., Cathey, W., "Extended depth of field through wave-front coding," Appl. Opt. 34, 1859-1866 (1995).

[10] Arnison, M., Cogswell, C. J., Sheppard, C. J. R. and Török, P., "Wavefront coding fluorescence microscopy using high aperture lenses," in [Optical imaging and microscopy: techniques and advanced systems, P. Török and F.-J. Kao, eds.], Springer-Verlag, Berlin,143-165 (2003).

[11] Prasad, S., Torgersen, T., Pauca, V., Plemmons, R., and van der Gracht, J., "High-resolution imaging using integrated optical systems", International Journal of Imaging Systems and Technology 14(2), 67–74 (2004).

[12] Conchello J. and Lichtman J., "Optical Sectioning Microscopy," Nature Methods 2(12), 920-932 (2006).

[13] Gibson, S. F. and Lanni, F., "Experimental test of an analytical model of aberration in an oil-immersion objective lens used in three-dimensional light microscopy," J. Opt.Soc. Am. A 9, 54–66 (1992).

[14] Preza, C., "Computational Optical Sectioning Microscopy Open Source (COSMOS) Software package", January 2014, http://cirl.memphis.edu/COSMOS

[15] Stockley, J. and Serati, S., "Cascaded one-dimensional liquid crystal OPAs for 2-D beam steering," Proc. 2003 IEEE Aerospace Conference 4, 1817-1822 (2003).

[16] Ronzitti, E., Guillon, M., de Sars, V., and Emiliani, V., "LCoS nematic SLM characterization and modeling for diffraction efficiency optimization, zero and ghost orders suppression," Opt. Express 20, 17843-17855 (2012)